Interaction of Polymethyl Methacrylate with Boehmite Filmed Aluminum Cladding under Gamma Irradiation

INL/JOU-24-76907
Revision 0

Advanced Test Reactor

OCTOBER 15, 2024

Daniel K. Sluder[a*],
Bryon J. Curnutt[a*],
Lorenzo Vega-Montoto [a*],
Joshua D. Orchard[a],
Matthew D. Horkley[a],
Trevor J. Skeen[a], and
Dean A. Stewart[a],

Idaho National Laboratory

Idaho National Laboratory

Battelle Energy Alliance manages INL for the U.S. Department of Energy's Office of Nuclear Energy

INL/JOU-24-76907
Rev. 0

Interaction of Polymethyl Methacrylate with Boehmite Filmed Aluminum Cladding under Gamma Irradiation

Daniel K. Sluder[a*], Bryon J. Curnutt[a*], Lorenzo Vega-Montoto [a*], Joshua D. Orchard[a], Matthew D. Horkley[a], Trevor J. Skeen[a], and Dean A. Stewart[a]
Idaho National Laboratory

October 15, 2024

Idaho National Laboratory
Idaho Falls, Idaho 83415

http://www.inl.gov

Prepared for the
U.S. Department of Energy
Office of Nuclear Energy
Under DOE Idaho Operations Office
Contract DE-AC07-05ID14517

Page intentionally left blank

SUMMARY

This paper presents an overview of ongoing work to qualify Advanced Test Reactor (ATR) driver fuel elements that were affected by irradiation degraded polymethyl methacrylate (PMMA) flux wands. Irradiation testing was performed on PMMA material in-contact with aluminum clad material. The cladding was prefilmed with a boehmite oxide layer, an important feature of ATR driver fuel. The effects on the boehmite layer due to gamma irradiation of the PMMA-Aluminum clad system were investigated. PMMA embrittlement, followed by softening and degradation occurred at high radiation levels. Adhesion between the cladding and irradiated PMMA was observed. Flow testing at prototypic ATR flow rates demonstrated effective removal of the adhered material. Measurements of the boehmite layer thickness were performed, and Raman spectroscopy was utilized to detect the presence of boehmite in the irradiated PMMA material.

Keywords: Cladding; Boehmite; Research Reactors; Material Interaction; polymethyl methacrylate

Page intentionally left blank

CONTENTS

SUMMARY v
ACRONYMS x
1. INTRODUCTION 12
2. INTRODUCTION 13
2.1. Materials 13
2.2. Irradiation Test 1 13
2.3. Irradiation Test 2 17
2.4. Raman Spectroscopy Measurements 18
3. RESULTS 18
3.1. Irradiation Test 1 18
3.2. Irradiation Test 2 20
3.3. Raman Spectroscopy Results 22
4. DISCUSSION 25
5. CONCLUSIONS 26
6. REFERENCES 26

FIGURES

Figure 1: Illustration of test samples. Control samples consisted of two cladding samples in contact with each other. Test samples consisted of two cladding samples in contact with a PMMA sample 13
Figure 2: ATR Cobalt Storage Bucket and test location. Test samples were irradiated in a high-intensity Co-60 gamma field 14
Figure 3: Flow attenuation test setup. Cladding samples with PMMA adherence were subjected to flow rates prototypic of ATR operating conditions 15
Figure 4: Change in boehmite oxide thickness at 109 rad for Irradiation Test 1 19
Figure 5: pH of Irradiation Vehicle Coolant 19
Figure 6: PMMA behavior at increasing exposure 20
Figure 7: PMMA attenuation during flow testing of sample 39 20
Figure 8: Change in oxide thickness for Irradiation Test 2 21
Figure 9: Visual images captured through a microscope equipped with a 20x lens. Image (A) displays the pristine plate serving as the control sample, (B) showcases the pristine PMMA also used as a control, (C) depicts the plate from Sample 24 subjected to heating and irradiation, and (D) illustrates the PMMA from Sample 24 after undergoing the same treatment 22
Figure 10: Average Raman spectra obtained using a confocal microscope outfitted with a 20x lens. The red line represents the spectrum of the pristine PMMA, serving as a control;

the green line corresponds to the spectrum of the pristine control plate; the magenta line depicts the spectrum of the plate from Sample 24 after heating and irradiation; and the blue line shows the spectrum of the PMMA from Sample 24 following the same treatment..... 23

Figure 11: This 3-D surface plots visualize the interaction between the irradiated polymer and plate by using the integrated intensity of specific peaks indicative of PMMA and Boehmite. Panel (A) reveals the irradiated plate with emphasis on the integrated intensity around the 2950 cm-1 peak, associated with PMMA. Panel (B) focuses on the same plate, highlighting the integrated intensity around the 2470 cm-1 peak, indicative of Boehmite. Similarly, Panel (C) illustrates the irradiated PMMA, concentrating on the integrated intensity around the 2950 cm-1 peak, while Panel (D) shows the irradiated PMMA with the integrated intensity around the 2470 cm-1 peak, again pointing to Boehmite.....24

TABLES

Table 1: Irradiation Test 1 Matrix.....16

Table 2: Irradiation Test 2 Matrix.....17

Page intentionally left blank

ACRONYMS

ATR	Advanced Test Reactor
DOE	U.S. Department of Energy
DOE-ID	U.S. Department of Energy-Idaho Operations Office
INL	Idaho National Laboratory
MFC	Materials and Fuels Complex
R&D	research and development

Page intentionally left blank

Interaction of Polymethyl Methacrylate with Boehmite Filmed Aluminum Cladding under Gamma Irradiation

1. INTRODUCTION

Aluminum alloys are widely used as cladding material at research and test reactors because of their high thermal conductivity and low neutron absorption cross-section. When exposed to air or water, aluminum alloys form an oxide corrosion layer due to oxidation. In a nuclear fuel system, the cladding acts as a protective barrier preventing the fission products being released into the environment. The oxide corrosion layers on aluminum clad fuels are beneficial as the oxide acts as a physical barrier between the cladding and the reactor coolant, preventing direct contact with the reactor coolant and reducing the rate of corrosion and erosion of the cladding. Performance of aluminum clad fuel is highly dependent on the presence and thickness of the oxide layer. Loss of the oxide layer due to spalling or mechanical damage can result in localized attack and corrosion of the aluminum cladding. Alternatively, uncontrolled oxide layer growth can result in increased fuel plate temperatures, thermal stresses, and buckling due to a lower thermal conductivity (Griebenow, Hansen, and Larrick, 1977). The type of aluminum oxide formed on the cladding affects fuel performance as well. The most important aluminum oxides for aluminum clad fuel are bayerite (α-Al(OH)3), and boehmite (AlO(OH)). Both Department of Energy (DOE) High Performance Research Reactors have a boehmite oxide layer on the fuel cladding, and the oxide layer is an important aspect of the fuel performance (J.C. Greiss, 1961). Advanced Test Reactor fuel is prefilmed with a boehmite layer by use of an autoclave, whereas a boehmite layer is formed on High Flux Isotope Reactor fuel during reactor operation (Greiss, 1961).

The oxide layer on aluminum-clad fuel is protected in several ways to ensure optimal fuel performance and safety. Primary coolant chemistry and fuel temperatures are highly controlled to prevent uncontrolled oxide growth or spallation. Physical inspections such as eddy-current measurements are often implemented to ensure oxide thicknesses are within limits, and rigorous handling procedures are implemented to prevent damage to the elements. Some evolutions, such as fuel channel cleaning, require intentional physical contact with the fuel element. A low-hardness material must be selected for such evolutions to protect the aluminum oxide layer. Polymethyl methacrylate (PMMA), and polyacrylates more generally, are commonly used in such nuclear applications (“Control of Detrimental Materials,” 1999). The absence of halogens, desirable mechanical properties, and a large body of literature detailing the effects of irradiation on PMMA make it a desirable material for nuclear use (Bruce and Davis, 1981) (Torrisi).

During the 2021 Core Internals Changeout (CIC) at the ATR, it was necessary to install fluence monitor wires into fuel coolant channels to map core power distribution as part of nuclear testing and core requalification. Wires of U-235 were attached to wands and inserted into the fuel element coolant channels to provide power measurement along the full axial length of the fuel plates. Impact modified PMMA was chosen as the flux wand material because the PMMA would not mechanically remove or damage the boehmite corrosion layer as a flux wand fabricated of metal would. Previously irradiated Cobalt-60 targets were installed in several experiment positions as reactivity shims, exposing some flux wands in the ATR driver fuel to higher levels of radiation than intended. Many of the flux wands became embrittled and broke apart during removal, and some flux wand material had reached exposure levels that resulted in the glass-transition temperature falling below the ambient temperature. Embrittled PMMA flux wand material was released into the ATR primary coolant, and several fuel elements had to be removed from service because of soft PMMA adhering to the cladding.

Irradiation testing was performed on the PMMA prior to its use, but the radiation levels seen during nuclear testing far exceeded the radiation levels during the preliminary testing of the PMMA. To support timely operation of the ATR, an updated investigation of PMMA in-contact with Boehmite filmed aluminum cladding under gamma irradiation was performed. The investigation studied PMMA behavior at different radiation levels, PMMA-cladding adherence, PMMA attenuation under prototypic ATR flow conditions, as well as Boehmite adherence and dissolution in PMMA. The findings of this investigation are reported in this paper.

2. INTRODUCTION

2.1. Materials

Two different sample types were constructed for this investigation: Control samples and test samples. Control samples consisted of two aluminum dummy fuel plates attached with an aluminum tie wire. The aluminum dummy fuel plates were fabricated from the same aluminum alloy used for ATR fuel elements and were boehmite pre-filmed using the same process applied to ATR fuel elements. Test samples consisted of a PMMA polymer suspended between two aluminum plates secured with an aluminum tie wire. Samples were either placed in an aluminum irradiation vehicle (Irradiation Test 1), or a borosilicate glass vial (Irradiation Test 2). To better simulate conditions that could be seen during ATR power operations, some sample assemblies were heated to 250°F (ATR driver fuel cladding surface temperature) for 2 hours prior to irradiation. Figure 1 provides an illustration of the test construction.

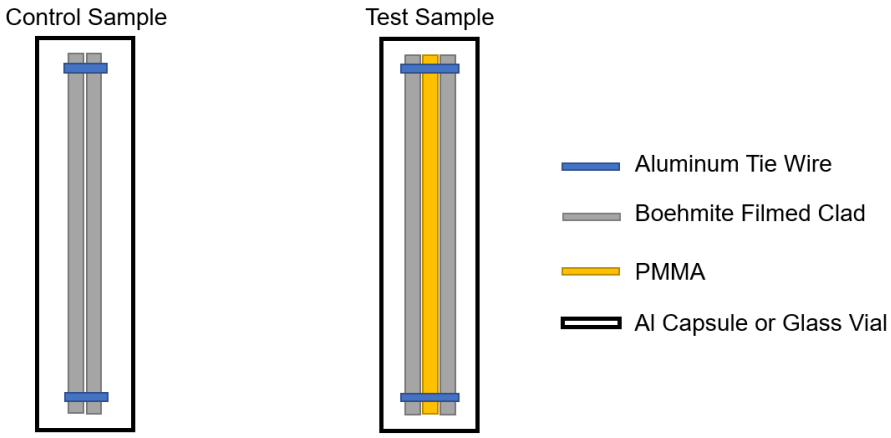

Figure 1: Illustration of test samples. Control samples consisted of two cladding samples in contact with each other. Test samples consisted of two cladding samples in contact with a PMMA sample.

ATR flux wands are fabricated from an impact modified PMMA based polymer sold as ACRYLITE Resist ZK-6. Test samples were cut from existing 0.042±0.004-inch-thick ATR flux wands sized to 1.75×0.5-inch rectangles with a 0.125-inch hole on each end for securing with the aluminum tie wire.

The aluminum under investigation in this experiment was constructed from an ATR dummy fuel element plate, specifically, a Boehmite pre-filmed plate type 19 with ID DUM-EE-01-14, which was procured from BWX Technologies, Nuclear Operation Group – Lynchburg. The plate was cut into 1.75×0.5-inch rectangles with a 0.125-inch hole on each end for securing with the aluminum tie wire. ATR plate type 19 is 0.100 + 0.00 / - 0.002 inches thick by 3.959 inches wide.

2.2. Irradiation Test 1

Irradiation Test 1 was performed in the ATR storage canal under conditions prototypic of the 2021 CIC core loading. One control sample, three preheated test samples, and eight standard test samples were

placed in an aluminum irradiation vehicle filled with ATR coolant water at a pH of 5.4. A 1/16th inch hole was drilled into the irradiation vehicles to prevent pressure buildup due to off gassing of the irradiated PMMA.

Test samples were placed underwater in the ATR Cobalt Storage Bucket for irradiation in a Co-60 spectrum. The ATR Cobalt storage bucket houses previously irradiated cobalt targets as illustrated in Figure 2. The test location had radiation fields that exceeded the upper range of 20.0 kR/hr of available radiation survey instrumentation used to perform underwater radiation measurements by Radiological Control personnel. Therefore, it was necessary to model the Co-60 capsules in spatial relation to an empirical exposure rate measurement within the range of available instrumentation. A calibrated Ludlum Model 9-7 high range ion chamber was used to obtain an underwater measurement of 16.5 kR/hr at the top of the ATR Cobalt Storage Bucket. Rate-to-Curie modeling with MicroShield was then used to determine the source strength at the test location. The nominal exposure rate at the test location was determined to be rad/hr. Total sample exposures were determined using this rate and the exposure time.

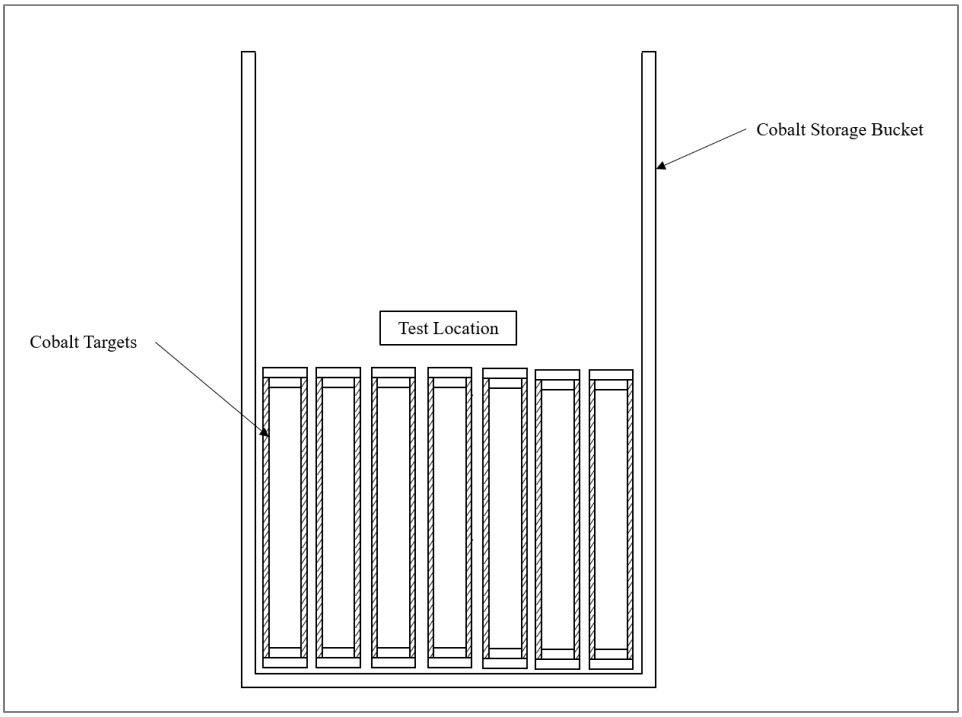

Figure 2: ATR Cobalt Storage Bucket and test location. Test samples were irradiated in a high-intensity Co-60 gamma field.

Preheated and standard experiment samples were removed and investigated at various exposure levels. Investigations performed were either visual, eddy current film thickness measurements, or flow attenuation tests. For each investigation, the pH of the irradiation vehicle water was measured then replaced with ATR Canal water at a pH of 5.4. Investigations performed, exposure levels, and sample types are provided in Table 1.

An investigator certified as a Level III Nondestructive Examiner (NDE) performed Eddy current film thickness measurements using a DeFelsko Poitector 6000 film thickness gauge. The gauge was zeroed to a clean, unirradiated dummy fuel plate cut from DUM-EE-01-08 prior to measurement. Film thickness measurements were then performed on the PMMA-facing side followed by measurements on the PMMA-diametric side.

pH measurements were performed using a Mettler Toledo SevenExcellence pH meter. After each irradiation period, water from all experiment capsules were poured into a lab vial and transferred to the

ATR chemist for measurement. The control sample was poured into a separate vial then transferred to the chemist for measurement.

Once PMMA-Cladding adherence was observed, samples were selected for flow attenuation testing. Flow attenuation testing was performed in the ATR canal at flow velocities nearly prototypic of ATR operation. Aluminum dummy plates with observed PMMA adherence were placed into a Ryerson T-2834 tube, and coolant was passed over the samples at velocities equivalent to those within ATR coolant channels during full power operation. Figure 3 illustrates the flow attenuation test setup.

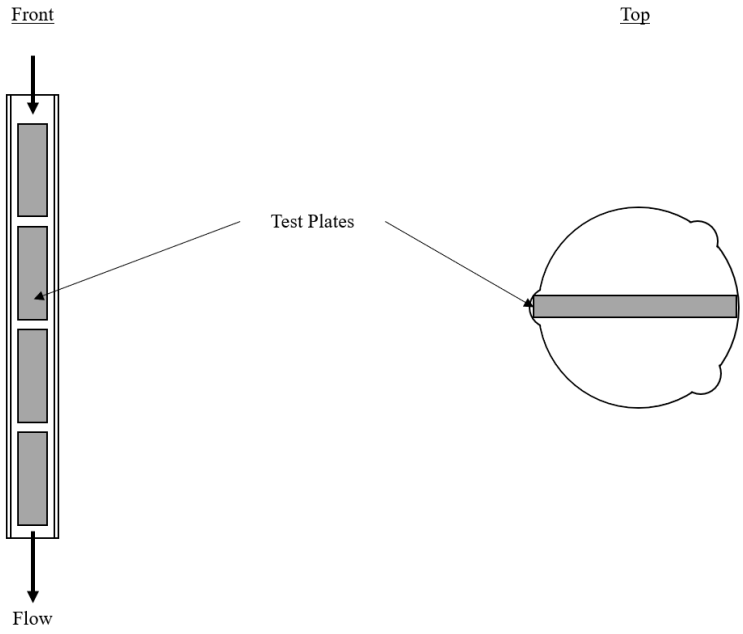

Figure 3: Flow attenuation test setup. Cladding samples with PMMA adherence were subjected to flow rates prototypic of ATR operating conditions.

Table *1*: Irradiation Test 1 Matrix

Sample ID	Type	Exposure (rad)	Investigations Performed
1	Control		Visual/Eddy Current
			Visual
			Visual/Eddy Current
			Visual
			Visual
2	Preheated		Visual/Eddy Current
			Visual
			Visual/Eddy Current
25	Preheated		Visual/Eddy Current
29	Preheated		Visual/Eddy Current
			Visual
			Visual/Eddy Current
30	Standard		Visual/Eddy Current
			Visual/Eddy Current
31	Standard		Visual/Eddy Current
			Visual
			Visual/Eddy Current
32	Standard		Visual/Eddy Current
			Visual
			Visual/Eddy Current
35	Standard		Visual/Flow Attenuation
36	Standard		Visual/Flow Attenuation
39	Standard		Visual/Flow Attenuation

2.3. Irradiation Test 2

Irradiation Test 2 was performed in a Foss Therapy Services Model-812 Cobalt-60 gamma irradiator at the Idaho National Laboratory. One control sample, four preheated test samples, and three standard test samples were placed in an air-filled borosilicate glass vials and irradiated at various exposure rates determined by laboratory personnel. Preheated and standard experiment samples were removed and investigated at various exposure levels. Investigations performed were either visual, eddy current film thickness measurements, or Raman spectroscopy of dummy plate surfaces and PMMA polymer material. Investigations performed, exposure levels, and sample types are provided in Table 2.

Table 2: Irradiation Test 2 Matrix

Sample ID	Type	Exposure (rad)	Investigations Performed
3	Control		Visual/Eddy Current
5	Standard		Visual/Eddy Current
6	Standard		Visual
7	Standard		Visual/Eddy Current
8	Standard		Visual
9	Standard		Visual/Eddy Current
10	Standard		Visual
11	Standard		Visual
12	Standard		Visual
13	Standard		Visual
14	Preheat		Visual
15	Preheat		Visual/Eddy Current
			Visual/Raman
16	Preheat		Visual
17	Preheat		Visual
18	Preheat		Visual
19	Preheat		Visual
20	Preheat		Visual
21	Preheat		Visual
22	Preheat		Visual/Eddy Current
23	Preheat		Visual/Eddy Current
24	Preheat		Visual/Eddy Current

			Visual/Raman

Eddy current film thickness measurements were also made using a DeFelsko Positector 6000 film thickness gauge. The gauge was zeroed to a clean, unirradiated dummy fuel plate cut from DUM-EE-01-08 prior to measurement. Film thickness measurements were then performed on the PMMA-facing side followed by measurements on the PMMA-diametric side.

2.4. Raman Spectroscopy Measurements

Raman micro-spectroscopic mapping measurements were conducted using a Senterra II Raman spectrometer (Bruker Optics) integrated with a BX-53M microscope (Olympus). The apparatus employed a 532 nm laser excitation source, focused onto the specimen through Olympus objective lenses. The utilized objective lens, featuring a 20x magnification and a numerical aperture (NA) of 0.40, resulted in a laser spot size of 5 μm. The scattered light collected by the objective lens was dispersed using a 400 grooves/mm grating and captured by a thermoelectrically cooled charge-coupled device (CCD) detector (Bruker Optics) at –60 °C. The experiments maintained a consistent laser power of 25 mW and employed integration times of 2 seconds with 6 co-averages. Background measurements corresponding to the integration times were collected for each dataset, culminating in a total spectrum collection time ranging from approximately 6 to 90 seconds. A spectral range of 500–3600 cm−1 was consistently utilized across all measurements, with excitation wavelength and wavenumber calibration internally conducted using a neon lamp before each session, achieving a spectral resolution of 4 cm−1.

The generation of Raman micro-spectroscopic mapping data entailed the use of rectangular grids, defined by size and location, to facilitate the collection of Raman spectra aligned with the dimensions of the analyzed grain. The strategy involved setting a ~50 μm step size between each collected spectrum within the grid. Specifically, grids were composed of 4 by 4 (16 total) Raman spectra. Both lateral and horizontal movements were precisely controlled via a motorized stage, with the height above the sample consistently maintained throughout the measurements. For high-resolution spectra acquisition, data collection was typically based on 400 total Raman spectra (arranged in a 20 by 20 spectral grid), with each spectrum integrated over 10 seconds and averaged across 3 co-averages.

Raman spectroscopy was performed on both PMMA and dummy plate test samples to investigate the presence of boehmite. Further, limited amounts of PMMA from the ATR CIC flux wands were removed from the primary coolant for investigation. PMMA samples were analyzed to identify the presence of boehmite within the material, while the dummy plate samples were analyzed to determine the presence of boehmite and PMMA. Boehmite exhibits a distinctive Raman peak at approximately 360 cm-1, which is indicative of its presence (Ruan, 2002).

3. RESULTS

3.1. Irradiation Test 1

As shown in Figure 4, the boehmite oxide layer appeared to be reduced following irradiation on the control plate and test plates. On test plates, a boehmite reduction appeared to occur on surfaces in-contact with the PMMA (PMMA adjacent) and surfaces not in-contact with the PMMA (PMMA diametric). Test samples which had visible PMMA adherence to the plate surface were excluded from this data. However, plates with PMMA visually adhered were measured and the PMMA thicknesses ranged from 5 μm to 325 μm. pH of the irradiation vehicle coolant was also observed to become more basic for the control sample and more acidic for the test samples as shown in Figure 5.

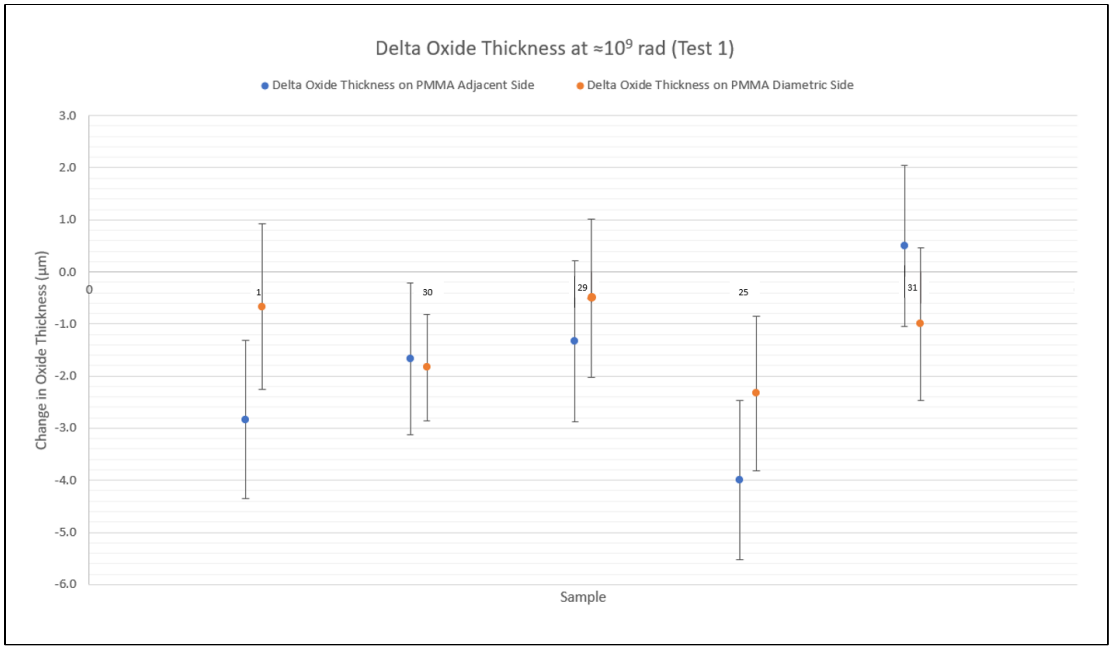

Figure 4: Change in boehmite oxide thickness at 109 rad for Irradiation Test 1.

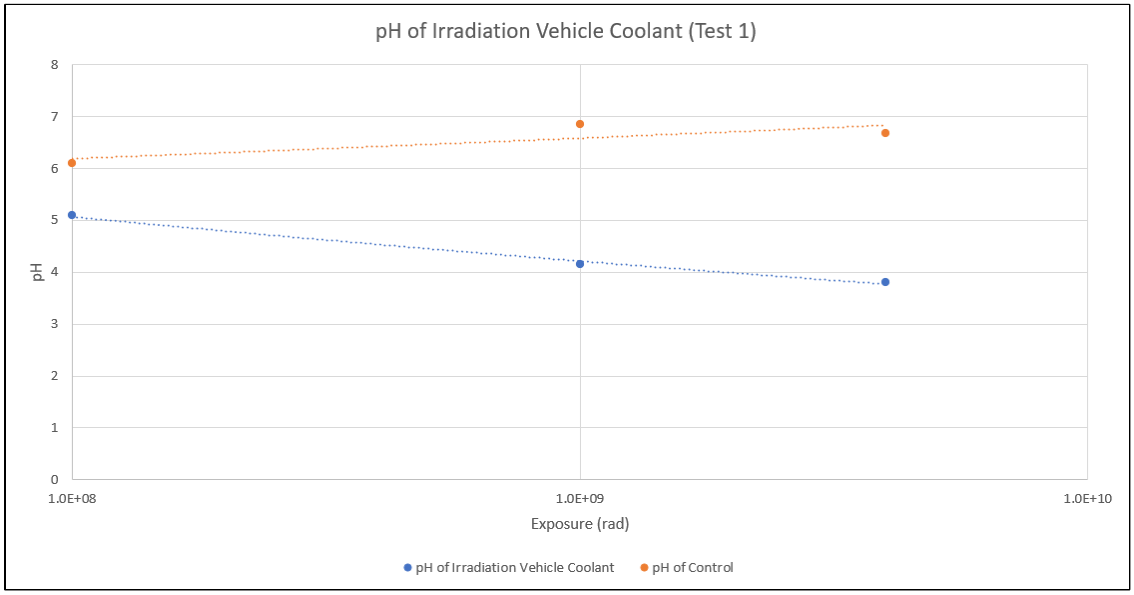

Figure 5: pH of Irradiation Vehicle Coolant.

The evolution of the PMMA polymer could be described in three phases as illustrated in Figure 6. At exposure levels between and rad, the PMMA was observed to become discolored and highly embrittled. No visible adherence of PMMA to the plates was observed at this exposure level. At exposures of approximately rad the PMMA was observed to have undergone significant swelling and bubbling. The PMMA was also reported to crumble easily and to have a rubbery feel, indicating that the polymer had a glass transition temperature at ambient room temperatures. A significant amount of PMMA-Aluminum adherence was observed at this exposure level. Preheat treatments of the samples were not observed to affect the amount of PMMA-aluminum adherence. At exposures levels between rad and rad, PMMA was observed to dissociate from the bulk material and recombine on all aluminum surfaces of the experiment, including the PMMA-diametric side of the plates and the irradiation vehicle. The bulk plastic material had expanded significantly and was still rubbery, indicating the glass-transition temperature was still at or below ambient room temperature.

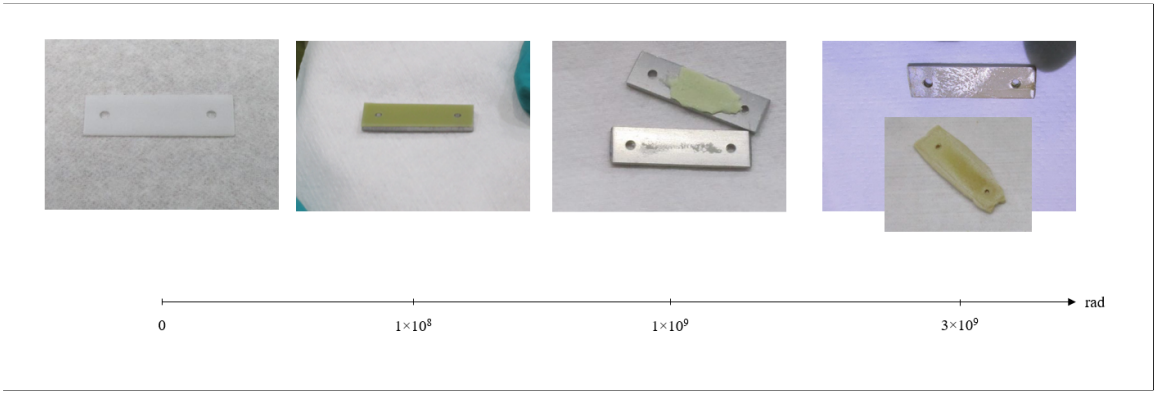

Figure 6: PMMA behavior at increasing exposure.

Plates with PMMA adherence and rad levels of approximately rad and rad were exposed to flow testing for approximately 300 seconds. For samples at rad, significant attenuation of PMMA was observed but visual amounts of PMMA were still adhered to the plate surface. Samples at higher levels of exposure (rad) were observed to have greater PMMA attenuation. Figure 7 shows attenuation of dissociated PMMA material on the PMMA diametric side of sample 39. While attenuation was significant, small amounts can still be observed on the plate.

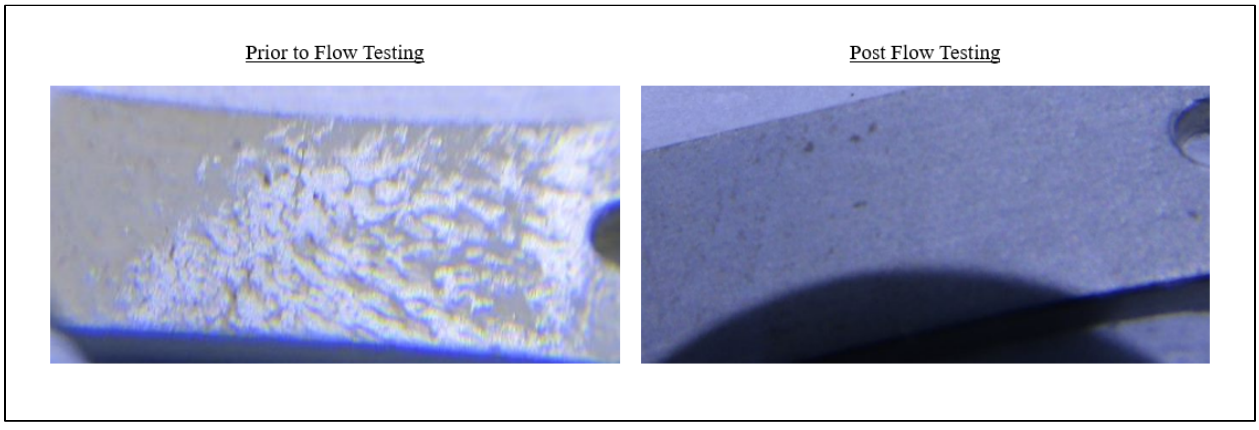

Figure 7: PMMA attenuation during flow testing of sample 39.

3.2. Irradiation Test 2

As shown in Figure 8, the boehmite oxide layer appeared to be reduced following irradiation on the test plates, whereas the control plate appeared to remain unchanged. On test plates, a boehmite reduction

appeared to occur on surfaces in-contact with the PMMA (PMMA adjacent) and surfaces not in contact with the PMMA (PMMA diametric). Test samples which had visible PMMA adherence to the plate surface were excluded from this data. The PMMA material evolution was similar to that of Irradiation Test 1. However, significant dissociation took place at lower rad levels.

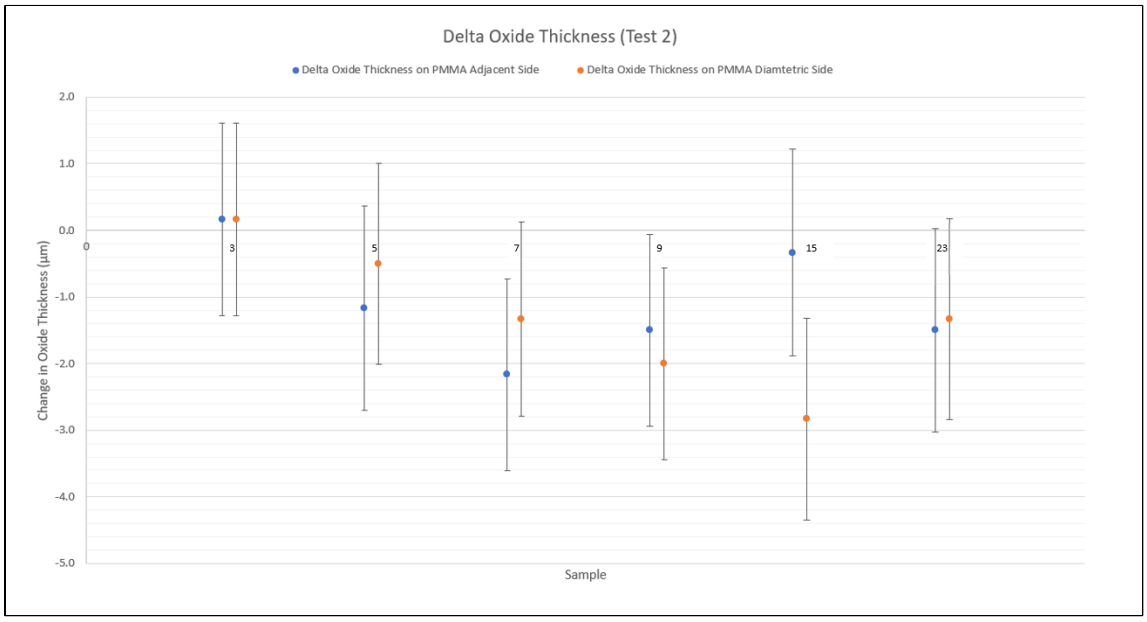

Figure 8: Change in oxide thickness for Irradiation Test 2.

3.3. Raman Spectroscopy Results

High-resolution visual images and Raman spectra were meticulously collected for pristine plates and PMMA separators, serving as control samples, in addition to heated and irradiated materials corresponding to Sample 24, utilizing a confocal Raman microscope. These critical data acquisitions provide a comprehensive insight into the structural and compositional changes across different conditions and materials. The collected visual images, which detail the morphological characteristics of each sample, are systematically presented in Figure 9.

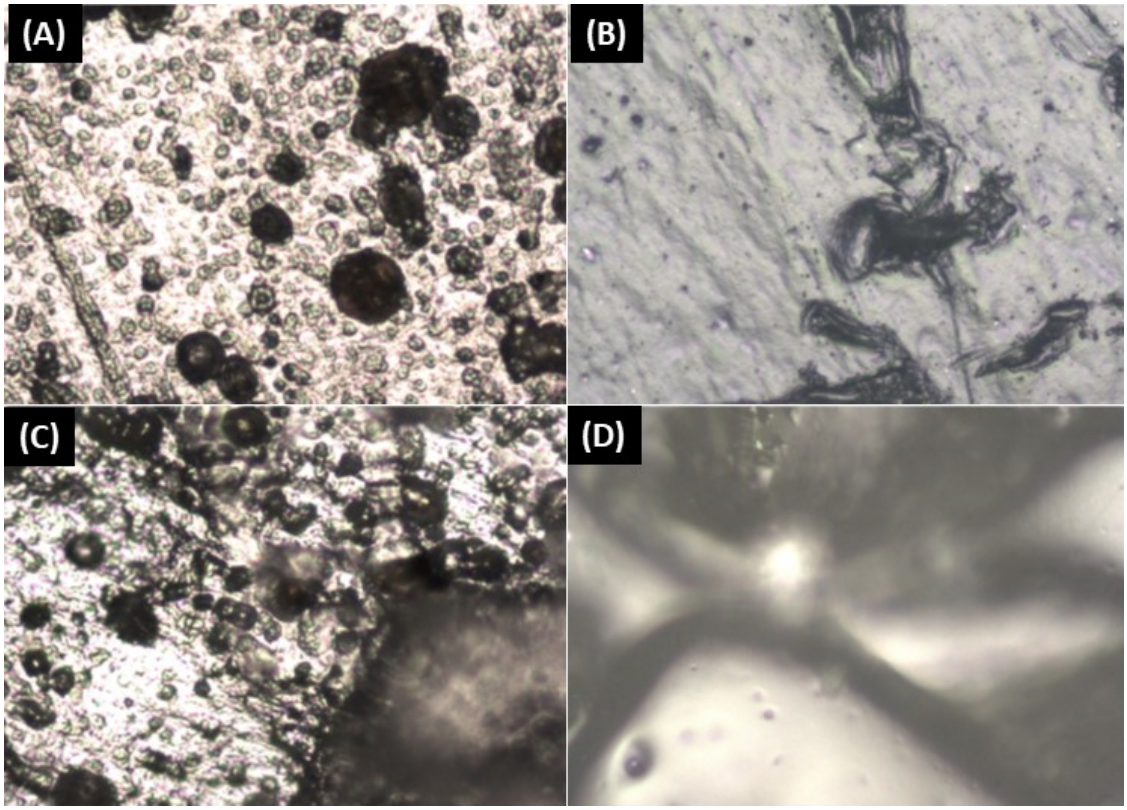

Figure 9: Visual images captured through a microscope equipped with a 20x lens. Image (A) displays the pristine plate serving as the control sample, (B) showcases the pristine PMMA also used as a control, (C) depicts the plate from Sample 24 subjected to heating and irradiation, and (D) illustrates the PMMA from Sample 24 after undergoing the same treatment.

Figure 10 displays the overlapping average Raman spectra for each material under various conditions, offering a qualitative assessment of the molecular vibrations and chemical compositions. This dual approach of combining high-resolution imaging with Raman spectroscopy enables a detailed analysis of the materials' responses to thermal and radiation stress, facilitating a deeper understanding of their behavior under extreme conditions.

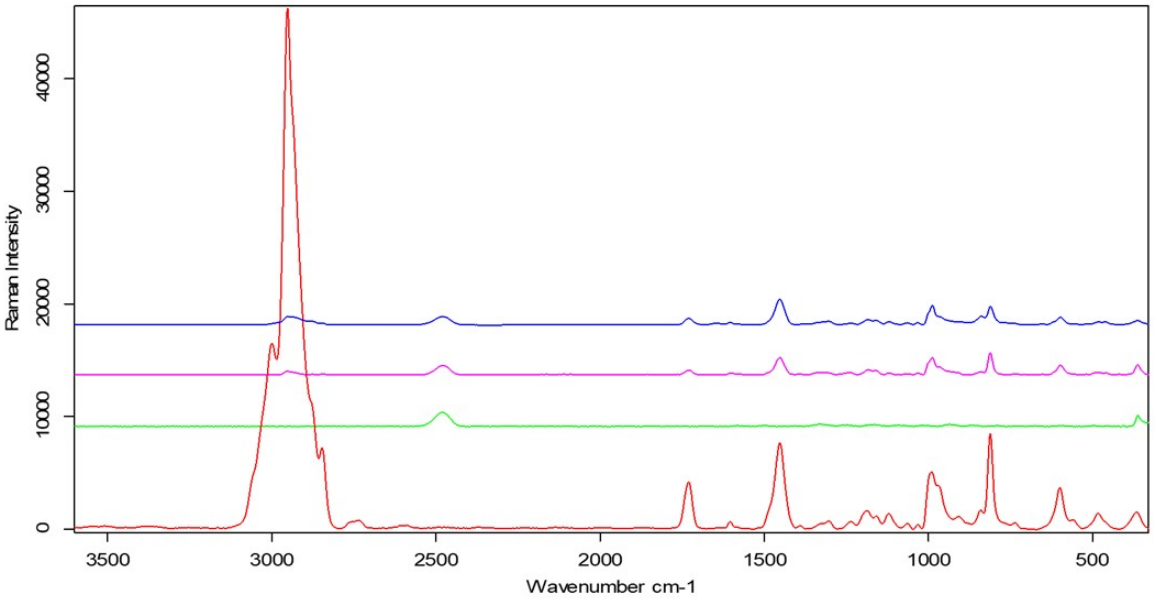

Figure 10: Average Raman spectra obtained using a confocal microscope outfitted with a 20x lens. The red line represents the spectrum of the pristine PMMA, serving as a control; the green line corresponds to the spectrum of the pristine control plate; the magenta line depicts the spectrum of the plate from Sample 24 after heating and irradiation; and the blue line shows the spectrum of the PMMA from Sample 24 following the same treatment.

Figure 11 presents the spectra obtained for the control plates and PMMA. Remarkably, the spectra for PMMA exhibited an almost perfect alignment with the reference spectra from the library for PMMA (results not shown for brevity). In contrast, the spectra for the plates were characterized by only two distinct peaks: one at 360 cm-1and another at 2470 cm-1. The peak at 360 cm-1 is recognized in scientific literature as a signature of Boehmite, which is noteworthy. However, it is important to mention that PMMA also displays a peak at this frequency, leading to potential overlap in spectral analysis. Despite thorough investigation, no literature reference could be identified for the peak at 2500 cm-1. Nonetheless, this peak was consistently observed in all samples of the plates, suggesting its significance in the material's spectral profile.

Figure 11 additionally showcases the average spectra for the components of Sample 24, which include the irradiated plate and PMMA. Remarkably, both spectra appear almost identical, illustrating spectral features characteristic of both the control plate and PMMA. This similarity unequivocally indicates an interaction between the components during the heating and irradiation process. The presence of shared spectral features not only confirms the physical and chemical interplay between the plate and PMMA under the applied conditions but also highlights the complex nature of these interactions. The spectra serve as a testament to the changes induced by the irradiation and heating treatments, providing valuable insights into the materials’ behavior and the resultant modifications to its molecular structure.

To further illustrate the interaction between the plate and PMMA, Figure 11 illustrates a 3-D surface plot of the irradiated polymer and plate, utilizing the integrated intensity of the peaks around 2950 cm-1 and 2470 cm-1 as indicators for the presence of PMMA and Boehmite, respectively. This graphical representation clearly demonstrates a correlative effect between these two peaks across the irradiated samples, providing strong evidence of material interaction. The peak at 2950 cm-1, typically associated with the vibrational modes of PMMA, and the 2470 cm-1 peak, indicative of Boehmite, both exhibit variations in intensity that suggest a mutual influence as a result of the irradiation process. This observation not only confirms the interaction between the materials but also offers insight into the extent and nature of the modifications that occur within the material's structure when subjected to such conditions. The 3-D surface plot serves as a powerful tool in visualizing these complex interactions, highlighting the dynamic changes in material composition and structure.

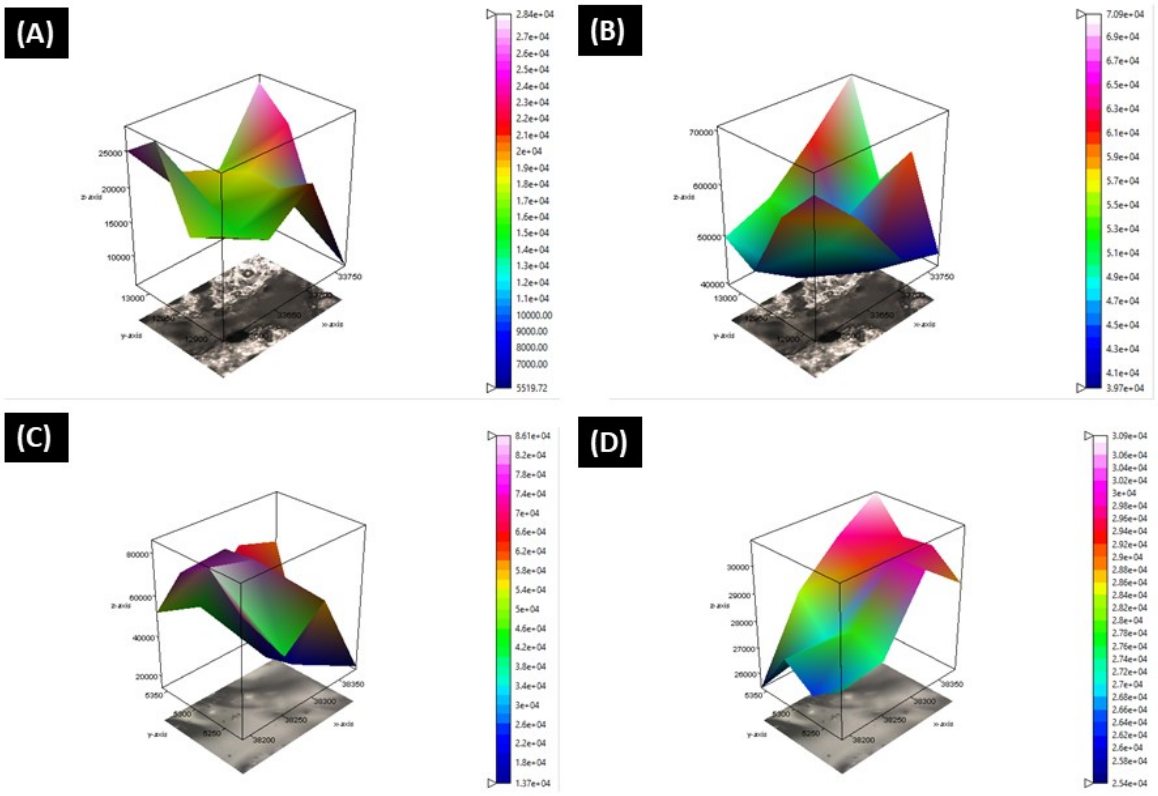

Figure 11: This 3-D surface plots visualize the interaction between the irradiated polymer and plate by using the integrated intensity of specific peaks indicative of PMMA and Boehmite. Panel (A) reveals the irradiated plate with emphasis on the integrated intensity around the 2950 cm-1 peak, associated with PMMA. Panel (B) focuses on the same plate, highlighting the integrated intensity around the 2470 cm-1 peak, indicative of Boehmite. Similarly, Panel (C) illustrates the irradiated PMMA, concentrating on the integrated intensity around the 2950 cm-1 peak, while Panel (D) shows the irradiated PMMA with the integrated intensity around the 2470 cm-1 peak, again pointing to Boehmite.

4. DISCUSSION

PMMA is an important material with many applications in the nuclear industry, particularly in research and test reactors. The chemical composition, mechanical properties, and radiation resistance make it a great candidate for many nuclear uses. Common uses include port covers, sight glass construction, flux wand material, and components of fuel handling tools. While the material offers a fair amount of radiation resistance for these applications, it is important to be cautious when the material can be exposed to high radiation fields for an extended period.

The material evolution of the PMMA observed in this experiment was consistent with existing literature. The dominant process of polymethacrylates under irradiation is chain scission (Torrisi). Scission is directly proportional to radiation exposure, producing methyl formate, methanol, and methyl methacrylate (Fox, Isaacs, and Stokes, 1963). Breakdown of the side-chains during scission released carbon monoxide and dioxide and hydrogen. Initially, these gases remained trapped in the polymer until the softening temperature was sufficiently lowered at higher levels of radiation exposure. Once the material was softened, these gases began to be increasingly released, and the "foaming" behavior described in *Breakdown of Methyl Methacrylate Polymer by High-Energy Radiation* was observed (Charlesby and Ross, 1953). Hydrogen and carbon dioxide release created an increasingly acidic environment in the irradiation vehicles. Macroscopically, high radiation fields will cause the material to evolve through three phases, as was observed in this work. These phases can be described as 1) embrittlement, 2) swelling and softening, and 3) breakdown and dissociation.

The embrittlement phase was seen at radiation exposure levels between and rad. During this phase, material interactions are not a significant concern because the gases resulting from chain scission are still trapped in the polymer. However, the mechanical properties of the material are greatly reduced during this phase. This can present a significant issue for tooling made of PMMA. Once in the embrittlement phase PMMA loses its ductility and tends to crack and crumble. Handling of tools or components made of PMMA in this phase can result in debris left in unwanted areas (e.g., in-tank). As a best practice, total exposure of PMMA in nuclear applications should be limited to levels below rad.

At radiation exposure levels nearing rad, the swelling and softening phase is observed. During this phase the PMMA material may continue to crumble, but the debris is much smaller than in the embrittlement phase. Once softening and swelling onsets, material interactions become relevant. The gases formed from chain scission begin to foam and release from the polymer. Local coolant chemistry may be affected and may become increasingly acidic. Further, the material tends to become sticky and may adhere to other components during this phase. The changing material properties and chemical evolution may present a challenge to many nuclear applications. As was found in this research, boehmite oxide may interact with PMMA during this phase. Boehmite provides passivation at 25°C for a pH range of 4.8 to 6.2 (M. Pouirbaix). As shown in Figure 5, total coolant pH dropped below the boehmite passivation range concurrent with the PMMA softening temperature being reduced to ambient temperature. At this point, localized changes in the coolant pH could have contributed to a reduced boehmite layer thickness. PMMA adherence and plating to the aluminum was also observed at this point, and some boehmite dissolution into the polymer took place as indicated by Raman spectroscopy. Despite the weep holes incorporated into the experiment design, a gas plenum had developed inside the irradiation vehicles. This correlated with the changing pH provides strong evidence that the gasses were formed and released from the polymer due to chain scission.

At radiation levels above rad, PMMA begins to dissociate from the bulk material and recombine on other surfaces. Local and global chemistry may be affected during this phase. PMMA dissolution and recombination can occur in a water or air atmosphere. If PMMA were to reach these exposure levels in a reactor environment, material recombination may affect fuel and the reactor vessel. The recombined material does not adhere well to surfaces, however, and may be easily removed. This experiment demonstrated that the prototypic ATR flow rate would efficiently remove recombined material.

5. CONCLUSIONS

The testing and results reported in this paper are directly in support of ongoing efforts to potentially qualify the impacted fuel elements for use in ATR. PMMA is seen as a useful polymer for contact tooling on an aluminum clad fuel system. However, material degradation must be prevented by controlling the radiation levels on the polymer. Material degradation becomes a concern at radiation levels above rad at standard temperature. Lower dose may create more rapid degradation at elevated temperature due to the products from radiolytic decomposition being more readily released as a result of weaker material properties at elevated temperatures. Once PMMA begins to degrade, it may interact with boehmite. Care should be taken to control radiation levels and ensure a PMMA-Boehmite interaction can be excluded.

6. REFERENCES

M. L. GRIEBENOW, G. H. HANSEN, and A. P. LARRICK, "TRA Oxide Film Control and Surveillance (A Reference Document)," INEL, RE&C Report RE-A-77-059 (Oct. 1977)

J. C. GREISS, et al., "Effect of Heat Flux on the Corrosion of Aluminum by Water. Part II. Influence of Water Temperature, Velocity, and pH on Corrosion-Product Formation," ORNL-3056 (Feb. 1961); https://doi.org/10.2172/4084602

GREISS, et al., "Effect of Heat Flux on the Corrosion of Aluminum by Water. Part III. Final Report on Tests Relative to the High-Flux Isotope Reactor," ORNL-3230 (Dec. 1961); https://doi.org/10.2172/4826330

"Control of Detrimental Materials," MIL-STD-2041, Revision D, August 5, 1999

M. B. BRUCE, M. V. DAVIS, "Radiation Effects on Organic Material in Nuclear Plants," EPRI-NP-2129 (Nov. 1981); https://doi.org/10.2172/5591289

L. TORRISI, "Ion Irradiation of Polymethylmethacrylate (PMMA)," Radiation Effects and Defects in Solids, 145, 4, 285-296; https://doi.org/10.1080/10420159808223996

H.D. RUAN, et al., "Far-infrared spectroscopy of alumina phases," Spectrochimica Acta Part A: Molecular and Biomolecular Spectroscopy, 58, 2, 265-272 (2002); https://doi.org/10.1016/s1386-1425(01)00532-7

R.B. FOX, L.G. ISAACS, S. STOKES, "Photolytic degradation of poly(methyl methacrylate)," J. Polym. Sci. A Gen. Pap., 1: 1079-1086 (1963); https://doi.org/10.1002/pol.1963.100010321

A. CHARLESBY, M. ROSS, "Breakdown of Methyl Methacrylate Polymer by High-Energy Radiation," Nature 171, 1153 (1953). https://doi.org/10.1038/1711153a0